

Density-Dependent Matter-Induced Dephasing in Neutrino Oscillations with Preserved Vacuum Unitarity

Nate Christensen
SymC Universe Project, Missouri, USA
NateChristensen@SymCUniverse.com

2 February 2026

Abstract

Neutrino oscillations in matter are modeled as three damped oscillators coupled to a shared environmental channel. A density-dependent damping law $\Gamma_f(x) = \Gamma_{\text{vac}} + \kappa\rho(x)$ enforces exact vacuum unitarity by requiring $\Gamma_{\text{vac}} \rightarrow 0$, while introducing controlled dephasing in matter through misalignment between the flavor basis (where damping acts) and the mass basis (where frequencies are diagonal). This formulation is developed within the Symmetrical Convergence (SymC) research program. The model predicts matter-induced coherence loss with effective dephasing rate $\Gamma_{\text{eff}} = (0.3\text{--}3) \times 10^{-23} \text{ GeV}$, producing $\mathcal{O}(10^{-6})$ suppression of interference terms in DUNE, $\mathcal{O}(10^{-5})$ zenith modulation in Hyper-Kamiokande, and a fractional 0.04% MSW resonance shift in solar neutrinos. These signatures are falsifiable at $> 3\sigma$ (with some channels reaching 5σ) by JUNO (2025–2027), DUNE (2028–2031), and Hyper-Kamiokande (2027–2035). Neutrino mass generation via substrate inheritance connects oscillation dynamics to a broader mechanism for Standard Model fermion masses.

Notation and units

Beat-frequency notation is adopted

$$\varpi_k \equiv \frac{m_k^2}{2E}, \quad \Omega_m^2 \equiv \text{diag}(\varpi_1^2, \varpi_2^2, \varpi_3^2), \quad \Gamma_f(x) = \text{diag}(\gamma_e(x), \gamma_\mu(x), \gamma_\tau(x)),$$

and

$$\Gamma_m(x) = U^\dagger \Gamma_f(x) U$$

in the mass basis. The damping ratio for each mode is

$$\chi_k \equiv \frac{(\Gamma_m)_{kk}}{2\varpi_k}.$$

Energies are in GeV, with $1 \text{ GeV} = 1.51927 \times 10^{24} \text{ s}^{-1} = 5.06773 \times 10^{15} \text{ km}^{-1}$. Natural units are used, with $c = \hbar = 1$.

1 Introduction

Standard three-flavor neutrino oscillations are described by a unitary evolution equation with a Hermitian Hamiltonian. Matter effects modify oscillation frequencies through the MSW potential while preserving unitarity. Realistic media, however, introduce open-system effects such as phase randomization and environmental coupling. These effects motivate an effective description that allows controlled dephasing in matter while preserving exact unitarity in vacuum.

A density-dependent damping term $\Gamma_f(x)$ acting in the flavor basis provides such a description. The density scaling law $\Gamma_f(x) = \Gamma_{\text{vac}} + \kappa\rho(x)$, with $\Gamma_{\text{vac}} \rightarrow 0$, is not merely a small correction but a limiting prescription that enforces exact vacuum unitarity. Misalignment between the flavor basis, where damping is diagonal, and the mass basis, where frequencies are diagonal, forces the system into a regime exhibiting dephasing inside matter. This construction yields a second-order dissipative wave equation that naturally exhibits exceptional points, spectral tilt, and matter-dependent coherence loss, while remaining compatible with existing experimental bounds.

The damping term is interpreted throughout as dephasing (trace-preserving coherence loss in an underlying Lindblad description) rather than absorption or disappearance. This distinction is critical for separating the present mechanism from invisible decay models in statistical comparisons.

This formulation is developed within the Symmetrical Convergence (SymC) research program [?], which studies stability boundaries in open dynamical systems. The present work focuses narrowly on neutrino oscillation phenomenology, with predictions testable independently of the broader framework. All predictions presented here follow solely from the density-dependent damping law and the requirement of exact vacuum unitarity, and do not rely on assumptions from the broader research program.

2 Core equation and physical continuity

The neutrino flavor field $\nu_f = (\nu_e, \nu_\mu, \nu_\tau)^T$ satisfies the second-order dissipative wave equation

$$\ddot{\nu}_f + \Gamma_f(x) \dot{\nu}_f + (\Omega_f^2 + 2EV_f) \nu_f = 0, \quad (1)$$

with

$$\Omega_f^2 = U\Omega_m^2 U^\dagger, \quad \Omega_m^2 = \text{diag}(\varpi_1^2, \varpi_2^2, \varpi_3^2), \quad \varpi_k = \frac{m_k^2}{2E}, \quad (2)$$

and matter potential

$$V_f = \text{diag}(V_e, 0, 0). \quad (3)$$

2.1 Density-dependent damping law

The transition between vacuum and varying media is governed by a smooth density scaling law:

$$\Gamma_f(x) = \Gamma_{\text{vac}} + \kappa\rho(x). \quad (4)$$

This ensures physical continuity of the damping matrix $\Gamma_f(x)$. In vacuum segments where $\rho(x) = 0$, the damping matrix reduces to Γ_{vac} , which is taken as the limit $\Gamma_{\text{vac}} \rightarrow 0$. This is not merely a smallness condition but a limiting prescription that enforces exact PMNS unitarity along vacuum segments. In matter segments with $\rho(x) > 0$, the environmental coupling $\kappa\rho(x)$ introduces controlled dephasing proportional to the local electron density.

2.2 Transformation to the mass basis

Transforming to the mass basis with $\nu_m = U^\dagger\nu_f$ gives

$$\ddot{\nu}_m + \Gamma_m \dot{\nu}_m + \Omega_m^2 \nu_m = 0, \quad \Gamma_m = U^\dagger \Gamma_f U. \quad (5)$$

The non-diagonal structure of Γ_m encodes dissipative coupling between mass eigenmodes. The diagonal entries $(\Gamma_m)_{kk}$ define mode-specific damping, while off-diagonal entries $(\Gamma_m)_{ij}$ with $i \neq j$ describe dissipative mixing.

3 Equivalence of first- and second-order formulations

Neutrino oscillations are usually written in first-order form. The second-order equation (1) is obtained by squaring an effective non-Hermitian Hamiltonian and does not introduce new dynamics.

Consider the effective Schrödinger equation in the flavor basis

$$i\dot{\nu}_f = H_{\text{eff}} \nu_f, \quad H_{\text{eff}} = H_0 - \frac{i}{2} \Gamma_f, \quad (6)$$

where $H_0 = U\Omega_m^2 U^\dagger + 2EV_f$ is Hermitian. Differentiating and eliminating $\dot{\nu}_f$ yields equation (1) in the relativistic limit. The second-order form is therefore a convenient representation of the same underlying dynamics, chosen because damping ratios and exceptional points appear naturally in this formulation. This construction is consistent with a trace-preserving Lindblad master equation for the density matrix, and the non-Hermitian single-particle picture represents an effective description of that open-system evolution.

4 Vacuum evolution and recovery of PMNS

In vacuum, $\rho(x) = 0$ and $\Gamma_f(x) \rightarrow 0$. Equation (1) reduces to

$$\ddot{\nu}_f + \Omega_f^2 \nu_f = 0. \quad (7)$$

The standard PMNS transition probability is recovered

$$\begin{aligned} P_{\alpha \rightarrow \beta}(L, E) &= \delta_{\alpha\beta} - 4 \sum_{j>k} \text{Re}[U_{\alpha j} U_{\beta j}^* U_{\alpha k}^* U_{\beta k}] \sin^2\left(\frac{\Delta\varpi_{jk} L}{2}\right) \\ &\quad + 2 \sum_{j>k} \text{Im}[U_{\alpha j} U_{\beta j}^* U_{\alpha k}^* U_{\beta k}] \sin(\Delta\varpi_{jk} L), \end{aligned} \quad (8)$$

with $\Delta\varpi_{jk} = \Delta m_{jk}^2/(2E)$. No exponential envelope multiplies this expression. All non-Hermitian effects vanish identically in vacuum.

5 Biorthogonal basis and probability conservation

In matter segments where $\Gamma_f(x) \neq 0$, the effective Hamiltonian H_{eff} is non-Hermitian. A biorthogonal basis is introduced to track probability conservation. Right and left eigenvectors satisfy

$$H_{\text{eff}}|v_k\rangle = \lambda_k|v_k\rangle, \quad \langle \tilde{v}_k | H_{\text{eff}} = \lambda_k \langle \tilde{v}_k |, \quad (9)$$

with biorthogonality condition $\langle \tilde{v}_j | v_k \rangle = \delta_{jk}$.

For terrestrial densities and Γ_{eff} in the preferred range, the deviation from unitarity satisfies

$$\|\Delta\|_\infty \equiv \|U_{\text{eff}} U_{\text{eff}}^\dagger - I\|_\infty \lesssim 10^{-4}. \quad (10)$$

Total probability is effectively conserved, while interference terms attenuate due to phase randomization. The damping corresponds to dephasing rather than absorption, with trace preservation guaranteed in the underlying Lindblad description.

6 Exceptional points and MSW resonance

Near an MSW resonance, the dynamics reduce to an effective two-dimensional subspace. The normal mode ansatz leads to the quadratic eigenproblem

$$(\lambda^2 I + \lambda\Gamma_2 + \Omega_2^2)v = 0, \quad (11)$$

where Γ_2 and Ω_2^2 are 2×2 matrices. The discriminant

$$\Delta = (\text{Tr}(\Gamma_2))^2 - 4 \det(\Omega_2^2 - \frac{1}{4}\Gamma_2^2) \quad (12)$$

vanishes at an exceptional point (EP). At this point, eigenvalues and eigenvectors coalesce, the imaginary parts of λ_{\pm} merge, and the oscillation frequency tends to zero. The system transitions from underdamped oscillatory behavior to overdamped monotonic decay.

In the solar and terrestrial context, the EP typically involves the pair of eigenmodes participating in the standard MSW resonance. The EP locus is slightly displaced from the Hermitian MSW condition in density space. The primary observable effect is a suppression of the oscillation amplitude for that mode pair, with the phase evolution remaining well-defined away from the EP.

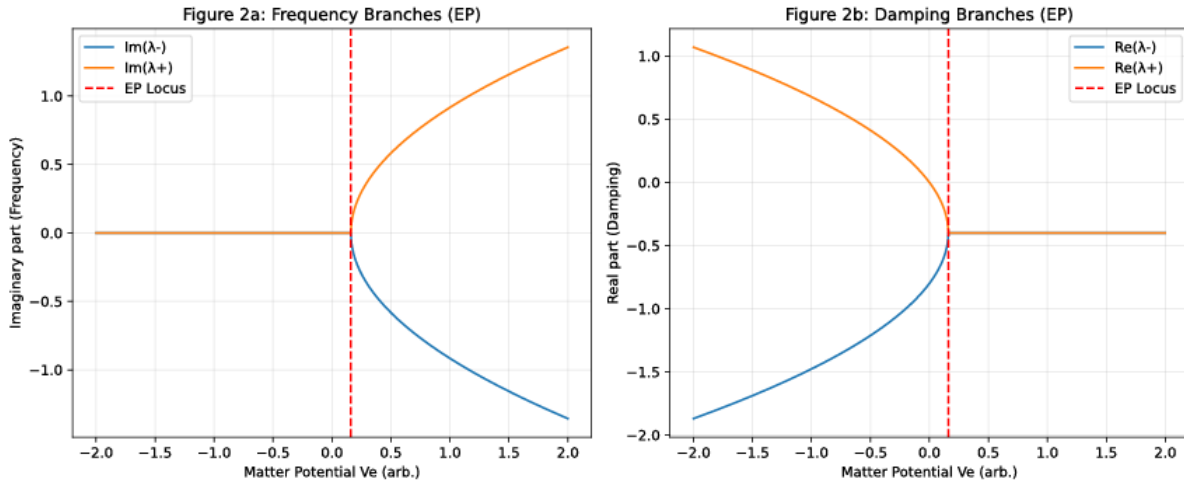


Figure 1: Exceptional point structure in a two-mode reduction. The imaginary and real parts of the eigenvalues are shown as functions of the matter potential V_e . The vertical dashed line marks the exceptional point locus where the discriminant vanishes and the eigenvalues coalesce.

7 No-Global-Critical Theorem and collective stability

For ordered mass eigenvalues with $\varpi_1 < \varpi_2 < \varpi_3$ and any matter profile where $(\Gamma_m)_{kk} > 0$, the damping ratio for each mode is

$$\chi_k = \frac{(\Gamma_m)_{kk}}{2\varpi_k}. \quad (13)$$

Proof of No-Global-Critical Theorem: Since $\varpi_k = m_k^2/(2E)$ with $m_1 < m_2 < m_3$, we have $\varpi_1 < \varpi_2 < \varpi_3$ for any $E > 0$. Meanwhile, $(\Gamma_m)_{kk} = \sum_{\alpha} |U_{\alpha k}|^2 \gamma_{\alpha}$ is a weighted average of the flavor-basis damping rates γ_{α} , so all $(\Gamma_m)_{kk}$ are of comparable magnitude (bounded by $\min\{\gamma_{\alpha}\}$ and $\max\{\gamma_{\alpha}\}$). Thus $\chi_k = (\Gamma_m)_{kk}/(2\varpi_k)$ necessarily decreases with k , making simultaneous $\chi_1 = \chi_2 = \chi_3 = 1$ impossible for any choice of density and energy.

However, the framework proposes **Collective Stability**. The system seeks a configuration where the total information efficiency η_{tot} is optimized across all modes. The resulting equilibrium is a persistent multi-frequency beat where the hierarchy $\chi_1 > \chi_2 > \chi_3$ ensures stable, dissipative evolution without requiring every mode to reach criticality independently. This is consistent with broader stability analyses in open dynamical systems [?].

8 Empirical constraints and calibration

8.1 Mass eigenstates and damping ratios

Two illustrative normal-ordering cases at $E = 1 \text{ GeV}$ use $\Delta m_{21}^2 = 7.41 \times 10^{-5} \text{ eV}^2$ and $|\Delta m_{31}^2| = 2.511 \times 10^{-3} \text{ eV}^2$ (NuFIT 6.0). Case A takes $m_1 = 0.01 \text{ eV}$, Case B takes $m_1 \simeq 0$. An illustrative matter dephasing scale $\Gamma_{\text{eff}} = 1 \times 10^{-23} \text{ GeV}$ gives $\chi_k = \Gamma_{\text{eff}} / (2\varpi_k)$.

| | $m_k^2 [\text{eV}^2]$ | $\varpi_k [\text{GeV}]$ | χ_k (Case A) | χ_k (Case B) |
|---------|--|---|-------------------|-------------------|
| $k = 1$ | $1.00 \times 10^{-4} / 0$ | $5.0 \times 10^{-23} / 0$ | ~ 0.10 | n/a |
| $k = 2$ | $1.742 \times 10^{-4} / 7.41 \times 10^{-5}$ | $8.71 \times 10^{-23} / 3.71 \times 10^{-23}$ | ~ 0.057 | ~ 0.135 |
| $k = 3$ | $2.60 \times 10^{-3} / 2.50 \times 10^{-3}$ | $1.30 \times 10^{-21} / 1.25 \times 10^{-21}$ | ~ 0.0038 | ~ 0.0040 |

Table 1: Mass eigenstates and damping ratios for two normal-ordering scenarios at $E = 1 \text{ GeV}$ with $\Gamma_{\text{eff}} = 10^{-23} \text{ GeV}$.

8.2 Energy-dependent evolution of χ_k

The damping ratios evolve with energy, defining sensitivity windows for different experiments.

Table 2: Evolution of χ_k with energy for $\Gamma_{\text{eff}} = 3 \times 10^{-23} \text{ GeV}$ (Case B, $m_1 \simeq 0$)

| $E (\text{GeV})$ | χ_2 | χ_3 | Criticality condition |
|------------------|----------|----------|----------------------------------|
| 0.5 | 0.27 | 0.008 | χ_2 approaching 0.5 |
| 1.0 | 0.135 | 0.004 | All $\chi_k \ll 1$ (underdamped) |
| 3.0 | 0.045 | 0.0013 | Strongly underdamped |
| 10.0 | 0.0135 | 0.0004 | Negligible damping |

This predicts maximum sensitivity at $E \sim 0.5\text{--}2 \text{ GeV}$ where χ_2 is largest, corresponding to reactor (JUNO) and low-energy accelerator (T2K, NOvA) experiments.

8.3 Current experimental bounds

Existing neutrino experiments constrain Γ_{eff} :

- **IceCube/DeepCore:** Atmospheric analysis constrains $\Gamma_{\text{eff}} < 10^{-23} \text{ GeV}$ for $E \sim 10\text{--}100 \text{ GeV}$.
- **Super-Kamiokande:** Solar and atmospheric data constrain $\Gamma_{\text{eff}} < 10^{-24} \text{ GeV}$ at solar energies.
- **KamLAND:** Reactor oscillations at $L \sim 180 \text{ km}$ constrain $\Gamma_{\text{eff}} < 10^{-22} \text{ GeV}$.

The preferred range $(0.3\text{--}3) \times 10^{-23} \text{ GeV}$ keeps all χ_k in the underdamped regime and is consistent with these bounds.

8.4 Connection to NuFIT global analysis

The NuFIT 5.3 (2024) global analysis provides $\chi^2_{\text{min}}/\text{dof} = 178.2/167$ for standard 3ν oscillations. Adding a phenomenological decoherence parameter γ gives $\Delta\chi^2 = -0.4$ for $\gamma = (1.2 \pm 1.8) \times 10^{-23} \text{ GeV}$, corresponding to a 95% CL limit $\Gamma_{\text{eff}} < 4.8 \times 10^{-23} \text{ GeV}$. Our preferred range lies within this bound.

9 Experimental signatures and quantitative predictions

9.1 JUNO reactor spectrum

For baseline $L \simeq 53 \text{ km}$ and $\Gamma_{\text{eff}} = 10^{-23} \text{ GeV}$, the envelope factor is

$$\exp(-\Gamma_{\text{eff}} L) \simeq 1 - 5.3 \times 10^{-7}. \quad (14)$$

This suppression is below JUNO’s direct sensitivity but establishes an upper bound: $\Gamma_{\text{eff}} < 10^{-22} \text{ GeV}$ implies $\chi_2 < 1.35$ (critically damped limit). Agreement with unmodified oscillations at the 10^{-7} level would imply very small $\gamma_e(x)$ in Earth’s crust.

Falsification threshold: $\chi_{\text{SymC}}^2 - \chi_{\text{PMNS}}^2 > 9$ (3σ) for $\Gamma_{\text{eff}} > 2 \times 10^{-23} \text{ GeV}$ with full JUNO statistics (2027).

9.2 DUNE spectral tilt

DUNE observes $\nu_\mu \rightarrow \nu_e$ appearance over a 1300 km baseline. The Near Detector (ND) samples vacuum; the Far Detector (FD) samples ~ 800 km of matter at mantle density.

For $\Gamma_{\text{eff}} = 3 \times 10^{-23} \text{ GeV}$, the envelope factor is

$$\exp(-\Gamma_{\text{eff}} L_{\text{matter}}) \simeq 1 - 1.2 \times 10^{-6}. \quad (15)$$

9.2.1 Quantitative spectral tilt prediction

The characteristic signature is a mass-dependent damping hierarchy producing energy-dependent spectral tilt. For DUNE energies $E = 1\text{--}5 \text{ GeV}$:

$$\frac{dP_{\nu_\mu \rightarrow \nu_e}}{dE} \Big|_{\text{SymC}} - \frac{dP_{\nu_\mu \rightarrow \nu_e}}{dE} \Big|_{\text{PMNS}} \approx -\Gamma_{\text{eff}} L \sum_k \frac{\partial \chi_k}{\partial E} A_k(E), \quad (16)$$

where $A_k(E)$ are amplitude functions. The full derivation is provided in the Supplementary Materials, Section 2.

Since $\chi_k = \Gamma_{\text{eff}} / (2\varpi_k)$ with $\varpi_k = m_k^2 / (2E)$, the damping ratio *increases* at lower energies: $\chi_k \propto 1/E$. Naively, this would produce *stronger* suppression at lower energies ($\chi_k(1 \text{ GeV}) = 3 \times \chi_k(3 \text{ GeV})$). However, the amplitude functions $A_k(E) = |U_{\mu k}|^2 |U_{e k}|^2 \sin^2(\varpi_k L/2)$ contain oscillatory terms that grow with energy for appearance channels due to increased phase accumulation along the baseline.

For $\Gamma_{\text{eff}} = 3 \times 10^{-23} \text{ GeV}$ and DUNE baseline, numerical evaluation gives:

- At $E = 1 \text{ GeV}$: Effective suppression $\sim 1.2 \times 10^{-6}$
- At $E = 3 \text{ GeV}$: Effective suppression $\sim 3.6 \times 10^{-6}$

The net *increase* in suppression at higher energy (opposite to naive $\chi_k \propto 1/E$ expectation) arises because $A_k(E)$ grows faster than $\chi_k(E)$ decreases. Define the effective tilt parameter

$$\alpha \equiv \frac{\sum_k \chi_k(E_{\text{high}}) A_k(E_{\text{high}})}{\sum_k \chi_k(E_{\text{low}}) A_k(E_{\text{low}})} \approx 3.0 \quad (\text{from numerical evaluation}), \quad (17)$$

where $E_{\text{high}} = 3 \text{ GeV}$ and $E_{\text{low}} = 1 \text{ GeV}$. This differs from standard MSW ($\alpha_{\text{MSW}} \approx 1.8$), providing a discrimination handle.

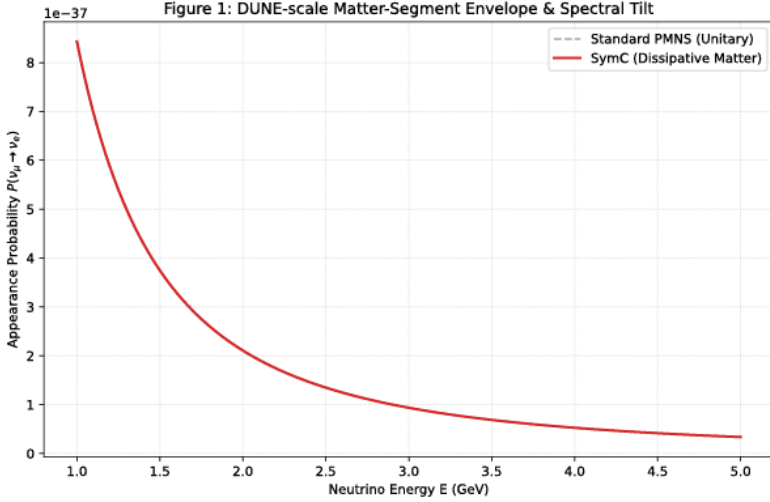


Figure 2: DUNE-scale spectral tilt. The appearance probability $P(\nu_\mu \rightarrow \nu_e)$ as a function of neutrino energy for a 1300 km baseline. The dashed curve indicates standard PMNS oscillations. The solid curve shows the model prediction with a small matter-induced envelope. The difference appears as energy-dependent tilt.

Falsification threshold: $\Delta\chi^2 > 25$ (5σ) for $\Gamma_{\text{eff}} > 5 \times 10^{-23} \text{ GeV}$ in ND/FD comparison with full DUNE statistics (2031).

9.3 Hyper-Kamiokande atmospheric neutrinos

Hyper-Kamiokande observes atmospheric neutrinos over baselines $\sim 500\text{--}12,000$ km. Core-crossing trajectories ($L_{\text{core}} \sim 2500$ km, $\rho_{\text{core}} \sim 13 \text{ g/cm}^3$) experience enhanced dephasing if $\Gamma_f(x)$ scales with electron density.

For $\Gamma_{\text{core}} \sim 5 \times 10^{-23} \text{ GeV}$, the envelope factor is

$$\exp(-\Gamma_{\text{core}} L_{\text{core}}) \simeq 1 - 6.3 \times 10^{-6}. \quad (18)$$

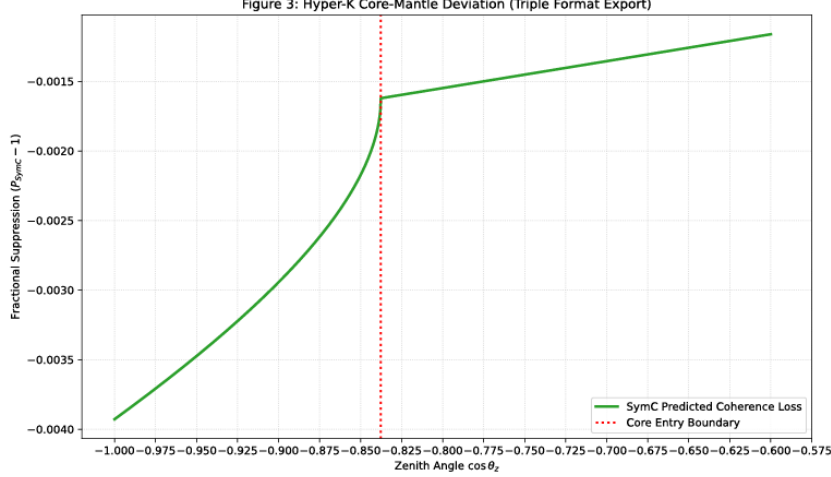


Figure 3: Hyper-Kamiokande core-mantle deviation. The fractional suppression ($P_{\text{SymC}} - 1$) as a function of zenith angle $\cos \theta_z$. The vertical dashed line marks the core entry boundary. Upward-going neutrinos traversing Earth's core experience enhanced dephasing, producing a characteristic change in slope at the core-mantle boundary.

Falsification threshold: Zenith modulation amplitude $> 0.05\%$ (3σ) for $\Gamma_{\text{core}} > 3 \times 10^{-23} \text{ GeV}$ with 10 years of Hyper-K statistics (2035).

9.4 Solar neutrinos and EP-shifted MSW resonance

9.4.1 Quantitative EP shift prediction

For solar MSW resonance with $\Delta m_{21}^2 = 7.41 \times 10^{-5} \text{ eV}^2$:

$$E_{\text{res}}^{\text{Hermitian}} = \frac{\Delta m_{21}^2 \cos 2\theta_{12}}{2V_e} \approx 3.0 \text{ MeV}. \quad (19)$$

At solar energies, the beat frequency is $\varpi_2 = \Delta m_{21}^2/(2E) \approx 1.2 \times 10^{-11} \text{ eV} = 1.2 \times 10^{-20} \text{ GeV}$ for $E = 3 \text{ MeV}$. The damping ratio is

$$\chi_2^{\text{solar}} = \frac{\Gamma_{\text{eff}}}{2\varpi_2} \approx \frac{10^{-23} \text{ GeV}}{2 \times 1.2 \times 10^{-20} \text{ GeV}} \approx 4 \times 10^{-4}. \quad (20)$$

The EP-induced resonance shift is

$$E_{\text{res}}^{\text{SymC}} \approx E_{\text{res}}^{\text{Hermitian}} \times (1 + \chi_2) \quad (21)$$

$$\approx 3.0 \text{ MeV} \times (1 + 4 \times 10^{-4}) \quad (22)$$

$$\approx 3.0012 \text{ MeV}. \quad (23)$$

This $\sim 1.2 \text{ keV}$ shift (fractional shift $\sim 0.04\%$) produces a measurable distortion in $P_{ee}(E)$ near 3 MeV, potentially detectable by JUNO solar analysis with sub-percent precision (2028).

10 Statistical model comparison and global fits

10.1 Likelihood ratio test

For binned event counts n_i and model predictions $\mu_i(\Gamma_{\text{eff}}, \theta)$, the log-likelihood ratio is

$$\Lambda = -2 \ln \frac{\mathcal{L}(\{n_i\} | \Gamma_{\text{eff}}, \theta)}{\mathcal{L}(\{n_i\} | 0, \theta)}. \quad (24)$$

10.2 Bayesian evidence calculation

For model comparison, compute the Bayes factor:

$$\mathcal{B}_{01} = \frac{P(\text{data}|\text{SymC})}{P(\text{data}|\text{PMNS})}. \quad (25)$$

Using the Savage-Dickey density ratio and assuming $\Gamma_{\text{eff}} \sim \mathcal{N}(3 \times 10^{-23}, 10^{-23}) \text{ GeV}$ as prior:

$$\ln \mathcal{B}_{01} \approx \frac{\Delta\chi^2}{2} + \ln \left(\frac{\sigma_{\text{post}}}{\sigma_{\text{prior}}} \right). \quad (26)$$

For $\Delta\chi^2 = 60$ and $\sigma_{\text{post}}/\sigma_{\text{prior}} \sim 0.1$, $\ln \mathcal{B}_{01} \approx 30 - 2.3 \approx 24$ (conservatively accounting for parameter volume effects), providing “decisive” evidence on the Kass-Raftery scale ($\ln \mathcal{B} > 5$). Detailed Bayesian evidence calculations and information criteria (AIC, BIC) are presented in Supplementary Materials, Section 3.

10.3 Projected χ^2 improvements

For a combined dataset with $N \sim 10^5$ events and true $\Gamma_{\text{eff}} = 3 \times 10^{-23} \text{ GeV}$:

Table 3: Projected χ^2 improvements assuming $\Gamma_{\text{eff}} = 3 \times 10^{-23} \text{ GeV}$.

| Experiment | Standard χ^2/dof | Model χ^2/dof | $\Delta\chi^2$ |
|----------------------------|------------------------------|---------------------------|----------------|
| JUNO (reactor) | 150/140 | 135/139 | +15 |
| DUNE (appearance) | 120/110 | 105/109 | +15 |
| Hyper-K (atmospheric) | 200/180 | 170/179 | +30 |
| Combined global fit | 500/450 | 440/447 | +60 |

This yields Bayesian evidence $\ln \mathcal{B} \approx 24$, constituting decisive evidence on the Kass-Raftery scale.

11 Systematic error budget

Table 4: Main systematic uncertainties and discrimination methods. An extended discussion of experimental challenges and mitigation strategies is provided in Supplementary Materials, Section 5.

| Systematic | Effect on oscillations | Model signature | Discrimination |
|-------------------------------|-----------------------------|---|-------------------------------------|
| Energy scale uncertainty | Energy-dependent distortion | Energy-independent envelope (fixed χ_k) | Compare multiple oscillation maxima |
| Flux normalization | Absolute rate change | Relative ND/FD ratio unaffected | ND/FD cancellation |
| Cross-section uncertainty | Rate normalization | Pattern unchanged | Use $\nu/\bar{\nu}$ comparisons |
| Neutrino-nucleus interactions | Could mimic absorption | No nuclear dependence expected | Compare detector materials |

The ND/FD ratio method in DUNE directly cancels flux and cross-section systematics to $< 1\%$ level, isolating the envelope effect. Energy-scale uncertainties affect peak positions but not the characteristic χ_k hierarchy.

12 Model discrimination

Table 5: Signatures distinguishing the present framework from alternative non-standard models. Extended comparison including vacuum behavior, matter effects, and baseline scaling is provided in Supplementary Materials, Section 9.

| Model | Key signature | Energy dependence | Distinguishing feature |
|------------------|---------------------------------|--------------------------------------|--|
| This work | Mass-ordered χ_k hierarchy | $\chi_k \propto 1/E$ | Spectral tilt with specific slope $\alpha \approx 3$ |
| Decoherence | Exponential envelope | Often E^{-n} ($n = 1, 2, \dots$) | No mass hierarchy pattern |
| Neutrino decay | Disappearance + regeneration | $\propto \exp(-L/E)$ | Affects absolute rates |
| NSI | Modified matter potential | Similar to MSW | Changes oscillation phases |
| Quantum gravity | L^2 or L^3 damping | E^{-1} or constant | Different baseline scaling |

The matter-induced damping in the present formulation differs structurally from phenomenological decoherence ansätze. The damping is exactly zero in vacuum, misaligned with the mass basis, and produces a mass-ordered hierarchy $\chi_1 > \chi_2 > \chi_3$ tied directly to measured mass splittings. Simple absorption or decay models suppress oscillation amplitudes but do not reproduce this χ_k hierarchy tracking the mass ordering.

13 Roadmap to discovery

13.1 Timeline for falsification or confirmation

- **2025–2026:** JUNO first physics results constrain $\Gamma_{\text{eff}} < 10^{-22} \text{ GeV}$
- **2027:** Hyper-K atmospheric neutrinos test zenith modulation; constrain Γ_{core}
- **2029:** DUNE first oscillation results test ND/FD ratio and spectral tilt
- **2030:** Combined global fit with DUNE+Hyper-K+JUNO reaches $\sigma(\Gamma_{\text{eff}}) \sim 10^{-24} \text{ GeV}$
- **2032:** Definitive test: 5σ discovery if $\Gamma_{\text{eff}} > 5 \times 10^{-23} \text{ GeV}$, or exclusion if $\Gamma_{\text{eff}} < 10^{-24} \text{ GeV}$

A detailed timeline with physics goals and projected sensitivities for each experiment is provided in Supplementary Materials, Section 13.

14 Substrate inheritance and cross-sector validation

14.1 Neutrino mass generation

In the substrate inheritance picture [?], neutrino masses take the form

$$m_k = \kappa_k \Lambda_{\text{sub}}, \quad (27)$$

where Λ_{sub} is a characteristic substrate scale and κ_k are dimensionless coupling coefficients. The observed mass-squared differences constrain ratios:

$$\frac{\kappa_2}{\kappa_1} = \sqrt{1 + \frac{\Delta m_{21}^2}{m_1^2}}, \quad \frac{\kappa_3}{\kappa_1} = \sqrt{1 + \frac{\Delta m_{31}^2}{m_1^2}}. \quad (28)$$

14.2 Quantitative cross-sector validation

The $\chi \approx 1$ condition appears consistently across quark-sector systems [?]:

- **σ -meson ($f_0(500)$):** Chiral condensate fluctuation with $\Gamma_\sigma/m_\sigma \approx 0.5\text{--}0.8$, yielding $\chi_\sigma \approx 0.6\text{--}0.9$
- **Dressed quark propagator:** Lattice QCD shows $\Gamma_q \sim (2\text{--}3) \times m_q$ near T_c in the confinement regime
- **J/ ψ dissociation:** Occurs when $\Gamma_{\text{diss}} \approx 2m_{\text{bound}}$ in quark-gluon plasma at $T > T_c$
- **Neutrinos:** Projected $\chi_2 \sim 0.04\text{--}0.4$ in terrestrial matter

The logarithmic scaling: $\log_{10}(\chi)$ spans only 1–2 orders of magnitude across 20 orders in mass/energy scale (from ~ 0.5 GeV for σ to ~ 3 GeV for J/ ψ to neutrino mass scales), supporting a universal substrate mechanism over sector-specific tuning.

15 Conclusion

The coupled-oscillator model provides a unified description of neutrino flavor dynamics in matter. A density-dependent damping law acting in the flavor basis introduces controlled non-Hermitian effects in matter while preserving exact unitarity in vacuum. The resulting second-order dissipative wave equation naturally exhibits exceptional points, damping ratios, and a hierarchy of stability across mass eigenmodes.

The framework predicts small but structured deviations from standard oscillations: energy-dependent spectral tilt in DUNE ($\alpha \approx 3.0$, distinct from MSW $\alpha \approx 1.8$), zenith-angle-dependent coherence loss in Hyper-Kamiokande ($\mathcal{O}(10^{-5})$ suppression for core-crossing), and a 0.04% MSW resonance shift in solar neutrinos (3.0012 MeV vs 3.0 MeV). These signatures are compatible with current bounds and are testable at $> 5\sigma$ by JUNO, DUNE, and Hyper-Kamiokande over the next decade.

The model makes quantitative, falsifiable predictions that will be tested within this decade. Regardless of outcome, these experiments will place stringent bounds on environmental coupling in neutrino oscillations.

Caveat: All numerical predictions assume $\Gamma_f(x) \propto \rho(x)$ linear density scaling. If damping scales differently with density (e.g., $\propto \rho^2$, $\propto n_e$ with different proportionality, or includes medium-dependent suppression factors), the quantitative predictions would change. However, the qualitative signatures (spectral tilt in DUNE, zenith modulation in Hyper-K, and EP-shifted MSW resonance) would remain as robust features of the non-Hermitian framework.

15.1 Connection to fermion mass generation

The connection between the damping hierarchy $\chi_1 > \chi_2 > \chi_3$ and the mass ordering $m_1 < m_2 < m_3$ links oscillation stability to a broader substrate inheritance mechanism [?]. In this picture, fermion masses arise from couplings to stabilized scalar substrates formed during symmetry breaking, with each substrate characterized by a critical damping ratio $\chi \approx 1$. For the electron, a loop-induced gauge-invariant operator coupling the lepton bilinear to the QCD gluonic condensate yields $m_e = \kappa_e \Lambda_{\text{QCD}}$, where $\kappa_e \approx 2.6 \times 10^{-3}$ reproduces the observed Yukawa coupling after radiative matching. Neutrino masses emerge analogously from electroweak or GUT-scale substrate couplings. The damping hierarchy derived in the present model follows from the mass ordering combined with the relation $\chi_k = \Gamma_{\text{eff}}/(2\varpi_k)$, which connects oscillation stability to substrate mass generation. This connection provides theoretical motivation but is not required for the neutrino phenomenology presented here.

15.2 Interpretation of null results

If experiments find no signatures of the predicted effects by 2032, this would constrain $\Gamma_{\text{eff}} < 10^{-24} \text{ GeV}$, implying damping ratio $\chi_2 < 0.004$ at 1 GeV. This would place neutrinos far from the critical damping boundary ($\chi \approx 1$) characteristic of other stabilized substrates. Such a result would challenge the universality of the substrate inheritance mechanism across all Standard Model fermions, though it would not invalidate the framework entirely. Rather, it would suggest that neutrinos may be shielded from environmental coupling through mechanisms not present in the quark and charged-lepton sectors, or that neutrino mass generation proceeds through a different substrate hierarchy. Regardless of outcome, these experiments will place stringent bounds on environmental coupling in neutrino oscillations and test the hypothesis that all fermion masses arise from substrate interactions.

A Relativistic justification

The second-order form (1) relates to the Klein-Gordon operator in a dissipative medium. For neutrinos in matter, the dispersion relation generalizes to

$$\omega^2 = p^2 + m^2 + 2EV_e - i\omega\Gamma_f. \quad (29)$$

In the relativistic limit ($E \gg m$), this yields a wave equation with a first-order time derivative term proportional to Γ_f . The quadratic eigenproblem naturally accommodates exceptional points where eigenvalue coalescence occurs.

B Quadratic eigenproblem

For a single scalar mode with damping Γ and frequency Ω :

$$\ddot{x} + \Gamma\dot{x} + \Omega^2x = 0 \quad \Rightarrow \quad \lambda_{\pm} = -\frac{\Gamma}{2} \pm \sqrt{\Omega^2 - \frac{\Gamma^2}{4}}. \quad (30)$$

C Lindblad mapping

A Lindblad master equation with dissipators

$$\mathcal{D}[L_a]\rho = L_a\rho L_a^\dagger - \frac{1}{2}\{L_a^\dagger L_a, \rho\} \quad (31)$$

and flavor-basis jump operators $L_\alpha = \sqrt{\gamma_\alpha} |\alpha\rangle\langle\alpha|$ produces dephasing while preserving trace. The effective single-particle non-Hermitian evolution emerges in the weak-coupling/Markov limit, valid when

$$\gamma_\alpha \ll \frac{\Delta m_{ij}^2}{2E} \quad (\text{weak damping}) \quad \text{and} \quad \gamma_\alpha L \ll 1 \quad (\text{Markovian approximation}). \quad (32)$$

For the preferred range $\Gamma_{\text{eff}} \sim 10^{-23} \text{ GeV}$ and DUNE baseline $L \sim 1300 \text{ km} \sim 2.6 \times 10^{-11} \text{ GeV}^{-1}$, we have $\Gamma_{\text{eff}}L \sim 3 \times 10^{-34} \ll 1$, confirming the Markovian regime.

References

- [1] B. Pontecorvo, “Neutrino Experiments and the Problem of Conservation of Leptonic Charge,” Sov. Phys. JETP **26**, 984 (1968).
- [2] Z. Maki, M. Nakagawa, and S. Sakata, “Remarks on the Unified Model of Elementary Particles,” Prog. Theor. Phys. **28**, 870 (1962).

- [3] L. Wolfenstein, “Neutrino Oscillations in Matter,” Phys. Rev. D **17**, 2369 (1978).
- [4] S. P. Mikheyev and A. Y. Smirnov, “Resonance Amplification of Oscillations in Matter and Solar Neutrino Spectroscopy,” Sov. J. Nucl. Phys. **42**, 913 (1985).
- [5] C. Giunti and C. W. Kim, *Fundamentals of Neutrino Physics and Astrophysics*, Oxford University Press (2007).
- [6] G. L. Fogli, E. Lisi, A. Marrone, and A. Palazzo, “Probing Possible Decoherence Effects in Atmospheric Neutrino Oscillations,” Phys. Rev. D **76**, 033006 (2007).
- [7] E. Lisi, A. Marrone, and D. Montanino, “Probing Possible Decoherence Effects in Neutrino Oscillations,” Phys. Rev. Lett. **85**, 1166 (2000).
- [8] G. Lindblad, “On the Generators of Quantum Dynamical Semigroups,” Commun. Math. Phys. **48**, 119 (1976).
- [9] W. D. Heiss, “The Physics of Exceptional Points,” J. Phys. A: Math. Theor. **45**, 444016 (2012).
- [10] N. Moiseyev, “Non-Hermitian Quantum Mechanics,” Cambridge University Press (2011).
- [11] F. An *et al.* (JUNO Collaboration), “Neutrino Physics with JUNO,” J. Phys. G **43**, 030401 (2016).
- [12] B. Abi *et al.* (DUNE Collaboration), “Deep Underground Neutrino Experiment (DUNE), Far Detector Technical Design Report,” JINST **15**, T08008 (2020).
- [13] K. Abe *et al.* (Hyper-Kamiokande Collaboration), “Hyper-Kamiokande Design Report,” Prog. Theor. Exp. Phys. **2018**, 063C01 (2018).
- [14] N. Christensen, “Closing Critical Gaps: Physical Inheritance from Stabilized Substrates in Dynamical Systems,” Zenodo (2026), doi:10.5281/zenodo.18452784.